Received: 9 March 2022 | Revised: 28 March 2022 | Accepted: 1 April 2022

DOI: 10.1002/jbio.202200070

RESEARCH ARTICLE

JOURNAL OF BIOPHOTONICS

Size-adjustable ring-shape photoacoustic tomography imager in vivo

Daohuai Jiang[1,2,3] | **Yifei Xu**[1] | **Hengrong Lan**[1,2,3] | **Yuting Shen**[1] | **Yifan Zhang**[1] | **Feng Gao**[1] | **Li Liu**[4*] | **Fei Gao**[1,5*]

[1]Hybrid Imaging System Laboratory, School of Information Science and Technology, ShanghaiTech University, Shanghai, China

[2]Chinese Academy of Sciences, Shanghai Institute of Microsystem and Information Technology, Shanghai, China

[3]University of Chinese Academy of Sciences, Beijing, China

[4]Department of Electronic Engineering, The Chinese University of Hong Kong, Hong Kong, China

[5]Shanghai Engineering Research Center of Energy Efficient and Custom AI IC, Shanghai, China

***Correspondence**
Fei Gao, Hybrid Imaging System Laboratory (HISLab), Shanghai Engineering Research Center of Energy Efficient and Custom AI IC, School of Information Science and Technology, ShanghaiTech University, Shanghai 201210, China.
Email: gaofei@shanghaitech.edu.cn

Li Liu, Department of Electronic Engineering, the Chinese University of Hong Kong, Hong Kong, China.
Email: liliu@cuhk.edu.hk

Abstract

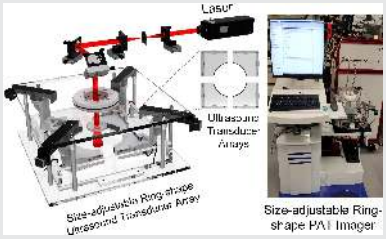

Photoacoustic tomography (PAT) has become a novel biomedical imaging modality for scientific research and clinical diagnosis. It combines the advantages of spectroscopic optical absorption contrast and acoustic resolution with deep penetration. In this article, an imaging size-adjustable PAT system is proposed for potential clinical applications such as breast cancer detection and screening, which can adapt to imaging targets with various sizes. Comparing with the conventional PAT setup with a fixed radius ring shape ultrasound transducer (UT) array, the proposed system is more flexible for imaging diverse size targets based on sectorial ultrasound transducer arrays (SUTAs). Four SUTAs form a 128-channel UT array for photoacoustic detection, where each SUTA has 32 elements. Such four SUTAs are controlled by four stepper motors, respectively, and can change their distribution layout position to adapt for various imaging applications. In this proposed system, the radius of the imaging region of interest (ROI) can be adjusted from 50 to 100 mm, which is much more flexible than the conventional PAT system with a full ring UT array. The simulation experiments using the MATLAB k-wave toolbox demonstrate the feasibility of the proposed system. To further validate the proposed system, imaging of pencil leads made phantom, ex-vivo pork breast with indocyanine green (ICG) injected, and in-vivo human wrist, finger and ankle are conducted to prove its feasibility for potential clinical applications.

KEYWORDS

image reconstruction, photoacoustic tomography, sectorial transducer array, size adjustable

1 | INTRODUCTION

In the female population, breast cancer is the most common Clinical research has demonstrated that early detection of breast cancer can significantly improve the 5-year survival rate of patients.[1] In view of limitations of the existing imaging modalities, new imaging techniques are required for accurate screening of early breast cancer. Such new imaging techniques need to overcome certain shortcomings of current methods, and desire: (1) nonionizing radiation;

Daohuai Jiang and Yifei Xu have contributed equally to this study.

(2) high sensitivity and specificity; (3) high repeatability; (4) low cost; (5) sufficient resolution; and (6) rapid imaging speed.

Photoacoustic Tomography (PAT) is an emerging noninvasive biomedical imaging method.[2–4] PAT combines the advantages of both optical contrast and acoustic penetration to achieve high-resolution functional and molecular imaging in biological tissues with unprecedented centimeter-level depth.[5, 6] In recent years, increasing studies have shown the potential of this technology to be used in pre-clinical and clinical applications.[7, 8] The principle behind PAT imaging is the photoacoustic effect. Specifically, when a laser beam is shot on biological tissues, the optical energy is absorbed by the tissues and converted into heat energy. Then, the photoacoustic signal caused by the thermal expansion of the biological tissue is produced, and propagates inside the tissue in the form of ultrasonic wave. The ultrasonic transducer is coupled with the biological tissue through the coupling agent to receive the PA signals, which can be used to reconstruct the optical absorption distribution within the tissue.

The PAT technique has been extensively studied for breast cancer detection. The typical imaging depth of PAT system for breast is ranging from 20 to 40 mm,[9] even larger depth of 70 mm with a portable photoacoustic breast imaging system was also reported in Reference 10. The main difference between the existing photoacoustic imaging systems involves the distribution layout of the ultrasound transducers. The conventional design of breast photoacoustic imaging systems can be divided into three types, that is, linear, planar and hemispherical.[11, 12] The linear distribution system typically uses a conventional handheld linear-array ultrasound probe with fixed optical fibers on either side of the transducer array for light illumination. It enables the breast to be illuminated and detected in the same direction.[6] Such design allows for easy exploration of the region of interest (ROI), but the system efficacy is highly dependent on the operator's skill due to the limited ROI. The planar distribution system clamps breast with two flat plates, allowing for detection with a 2D array of transducers.[13] Such method yields a larger field of view with fewer artifacts, but it is difficult to obtain an overall view near the chest wall. The hemispherical distribution system allows for a complete 3D scan of the breast by mounting a dense array of ultrasound transducers in a bowl shape.[14] Design scheme that can achieve similar performance by rotating a linear array was reported as well.[15] This design provides the largest number of detection angles, suffering the least from artifacts and allowing for a larger field of view. However, the use of a considerable number of transducers makes both data acquisition and processing challenges, often requiring longer reconstruction times and higher costs. So far, PAT-based clinical diagnosis has been achieved for breast cancer detection, but the existing systems still have problems to be addressed, when taking the specific application scenario into consideration such as rapid screening of breast cancer. One disadvantage is that these systems do not take the diversity of breast sizes into consideration, which may severely hamper the performance of breast imaging.

In this article, we designed a rapid breast screening PAT system based on size-adjustable sectorial ultrasound transducer arrays (SUTAs), which has substantial improvement compared with our previously published study.[16] The system incorporates four separated SUTAs, whose position can be adjusted by four stepper motors to provide high-resolution rapid screening for a larger scale population. Specifically, we demonstrated the ROI size-adjustable PAT system in simulation, phantom study, ex-vivo experiments and human in-vivo wrist and ankle validation. The proposed system can adapt for different-size imaging targets, and enhance the versatility of the PAT system for clinical applications.

The remainder of this article is organized as follows: Section 2 will introduce the method of the SUTA-based ROI size-adjustable PAT system including the transducer array design, SUTA distribution layout, and imaging reconstructions. In Section 3, both simulation, ex-vivo and in-vivo experiments are conducted to assess the feasibility of the size-adjustable PAT system. Sections 4 and 5 present discussions and conclusions for the proposed PAT system.

2 | METHOD

2.1 | Overview

In this article, a size-adjustable PAT system was proposed to adapt to a variety of sizes of imaging targets. The ultrasound transducer in this system is different from the conventional ring array with a fixed radius or the linear array. A sectorial ultrasound transducer with size-adjustable capability was designed to obtain better PA signals from different size imaging targets.

Figure 1 shows the overview of the system workflow. The laser source excites the imaging target and then generates PA wave; the computer controls the stepper motors that change the distributions of the four SUTAs; the PA signals received by the SUTAs are sampled by the data acquisition (DAQ); after that, the computer reconstructs the PA image by applying the back-projection (BP) algorithms and the model-based (MB) algorithms.[17]

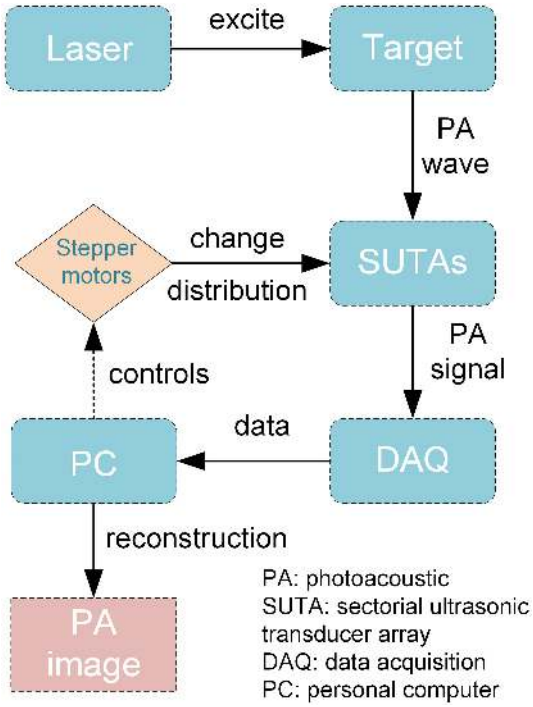

FIGURE 1 The overview of the size-adjustable PAT system workflow

The stepper motors drive the four SUTAs to move towards the imaging target, ensuring that the transducer can better receive the PA signals with compact enclosure. For image reconstruction, the coordinates of the ultrasonic transducer elements of the SUTAs are necessary. Based on the stepper motors' movements and the shape of SUTA, the coordinate of each transducer element can be uniquely calculated for image reconstruction. Therefore, the proposed system using the SUTAs can achieve size-adjustable ROI for PAT imaging.

2.2 | Sectorial ultrasound transducer array design

The ultrasound transducer is an essential component of the PAT system for PA wave detection.[18] To reconstruct a high-fidelity PA image, the PA signals should be received at full angles. Thus, for the conventional PAT system setup, a ring-shaped UT array with full-angle ultrasound transducer (UT) elements distribution is preferred to receive the PA signals for image reconstruction. In this article, we proposed a sectorial shape UT array for PA wave detection. Figure 2 shows the 3D plot of the custom-designed SUTA structure. The PA signal is detected by four SUTAs with a 90-degree interval in a plane that forms a ring-shaped UT array. The four SUTAs distribution can be flexibly changed according to the

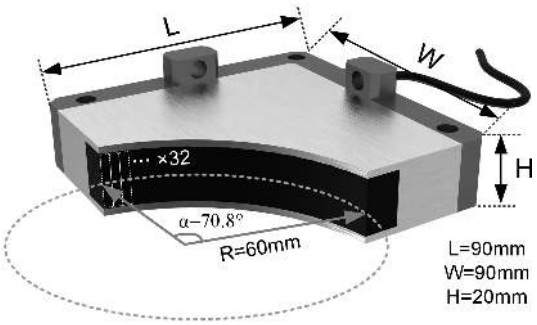

FIGURE 2 The proposed SUTA schematic diagram. L, length; W, width; H, height; R, radius

different imaging targets. The dimension of the SUTA is shown in Figure 2. The SUTA with an axial symmetry shape has a length equal to the width of 90 mm, and the height is 20 mm. For each SUTA, there are 32 elements for ultrasound detection, which evenly distribute on the sector arc with a radius of 60 mm. Each element is 2.317 mm in width and 10 mm in height. The degree of the sector arc is 70.8° for ultrasound detection. Therefore, by applying four SUTAs, it can form a 128-channel size-adjustable UT array.

Because photoacoustic signal is a broadband signal, to get a detailed reconstructed image, more frequency component needs to be captured.[5, 7] Therefore, four kinds of SUTA with different center frequencies are designed in this study. We selected 7.5, 5, 2.5 and 1 MHz as center frequency for each SUTA with 60% bandwidth, which can cover the PA signals' spectrum for most PAT system applications.

2.3 | SUTA's distribution with ROI size-adjustable

In this study, the ultrasound detection part of the PAT system is the four SUTAs based 128-channel transducer array, each SUTA's position can be flexibly changed for better PA signal detection. Therefore, changing the four SUTAs distribute position for PA signal receiving can realize an ROI size-adjustable PAT imaging. As shown in Figure 3A–C, they demonstrate the three situations that the four SUTAs form a 128-channel array for PA signals detection.

For the small target, the ultrasound transducer close to the PA wave source can get better detection sensitivity that avoids the severe acoustic attenuation during the propagation. Therefore, the four SUTAs close to the imaging center can form a small region for PA signals detection as shown in Figure 3A. Changing the SUTAs position can adapt for imaging targets with various sizes,

as shown in Figure 3B,C, which can be used for imaging middle and large targets. Figure 3D is the photograph of the four SUTAs controlled by four stepper motors. Therefore, by controlling the stepper motors' movements, the size of the ROI is changed correspondingly. To get better control and PA signal processing, the four stepper motors' movements are towards the imaging field center. For better quantitative analysis of the size-adjustable PAT system, we defined the parameter a, which quantified the distance between the adjacent SUTA, as shown in Figure 3B. When the SUTAs formed a standard circular distribution, the parameter a is defined as a_0. Specifically in this system, the a_0 is 20 mm.

The ROI of the four SUTAs based PAT system can be approximated as the inscribed circle shown in Figure 4. Figure 4A shows the situation that the SUTAs formed a small region for PA signals detection, the parameter a satisfied the relationship of $0 \le a \le a_0$. In this case, the inscribed circle is always tangent to the middle of the arc

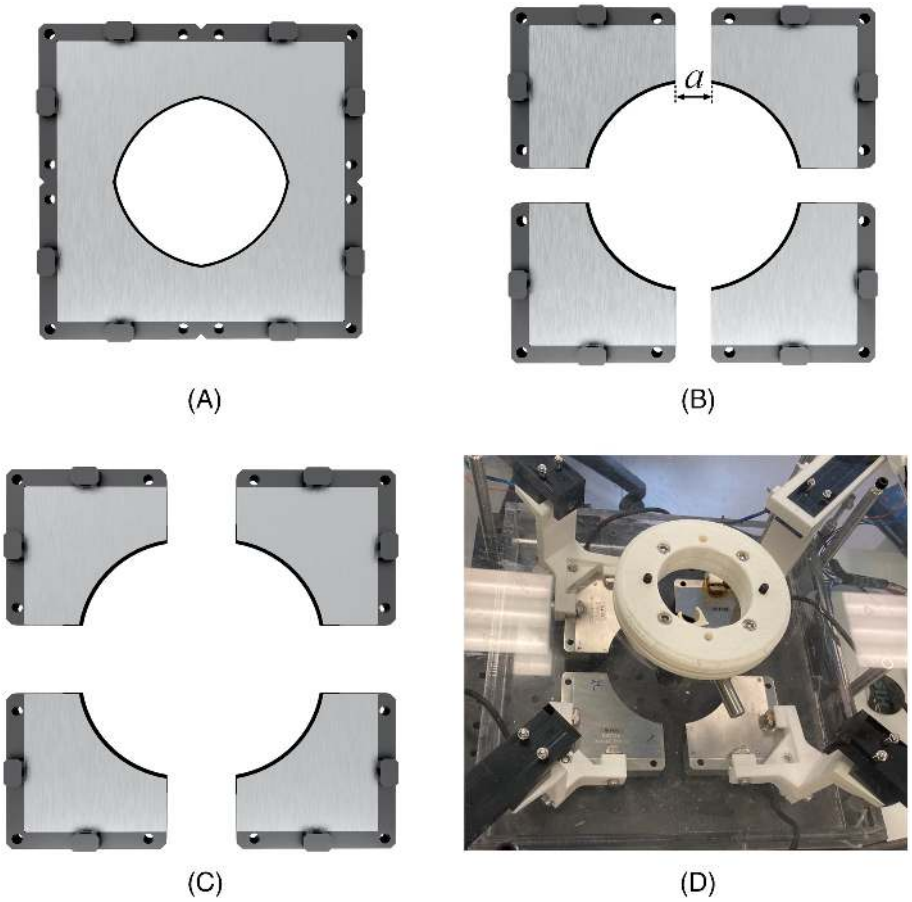

FIGURE 3 The ROI size-adjustable PAT system with four SUTAs. (A) is the situation for small ROI with 50 mm radius, (B) forms a middle size region with 60 mm radius and (C) is for large ROI; (D) the photograph of the four SUTAs' distribution controlled by stepper motors

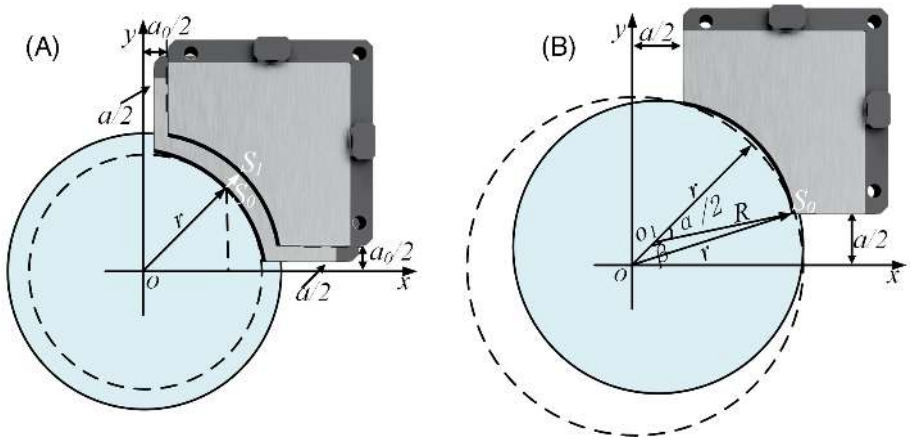

FIGURE 4 The radius of the inscribed circle calculation model for the ROI of the SUTA-based PAT system. (A) the SUTAs for the small region for signals detection ($0 \le a \le a_0$), o is the center of the imaging region, S_0 is the tangent point of the small imaging region circle to the SUTA arc; (B) the SUTAs formed a large region for PA signals detection ($a \ge a_0$), o is the center of the large imaging region, o_1 is the center of the SUTA arc

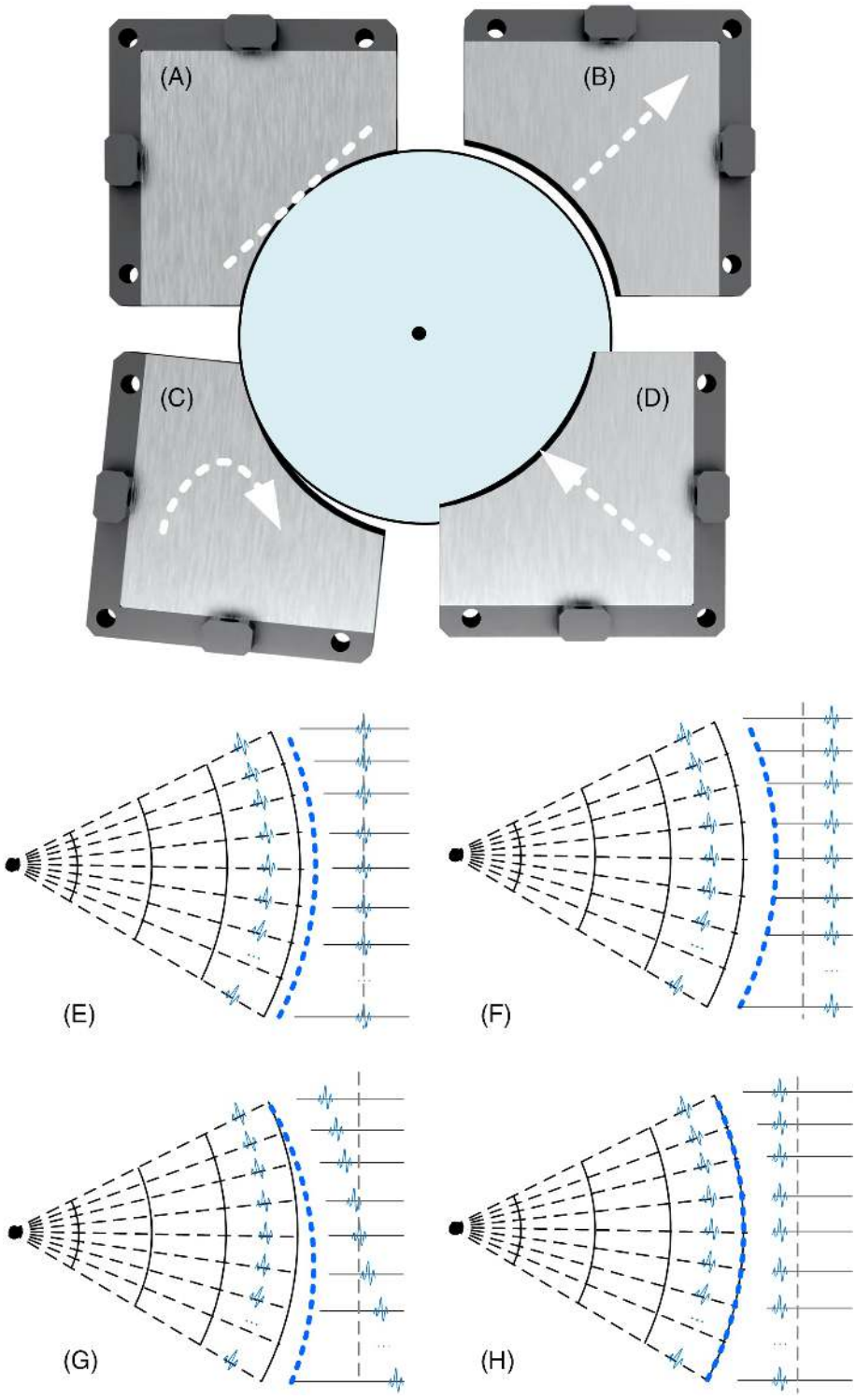

FIGURE 5 The four SUTAs distribution diagram with position error. (A) The SUTA is distributed towards the center of the imaging area with no offset errors; (B) the SUTA is distributed towards the center of the imaging area with backward offset error; (C) the situation of SUTA is not oriented towards the center of the imaging area; (D) the SUTA is distributed towards the center of the imaging area with forwarding offset error; (EH) are the calibration signals situation corresponding to the SUTA with (A–D) distribution, respectively

of the SUTA, then the radius r of the inscribed circle can be easily calculated by subtracting the length between S_0 and S_1 from the arc radius R of SUTA. When the SUTAs formed a large region for PA signals detection ($a > a_0$), as shown in Figure 4B, the radius of the inscribed circle can be calculated by the *cosine low* in the triangle of Δoo_1S_0. Therefore, the radius r of the inscribed circle can be calculated by the formula as:

$$\begin{aligned} r &= R - \frac{\sqrt{2}}{2}(a_0 - a) && 0 \le a \le a_0 \\ r &= \sqrt{\frac{1}{2}(a-a_0)^2 + R^2 - \sqrt{2}R(a-a_0)\cdot\cos\beta} && a > a_0 \end{aligned} \quad (1)$$

where β is the angle determined by π-$\alpha/2$, the α is the degree of SUTA arc, that is, 70.8° in this article.

The proposed SUTA-based ROI size-adjustable PAT system can easily realize the radius ranging from 50 to 100 mm for PA signals detection with high flexibility.

However, the gap between SUTAs increases, along with the ROI size enlargement. Therefore, for large ROI imaging, there is still a limited view issue, which can be solved by rotational compensation.

2.4 | SUTA signal calibration and image reconstruction

The four SUTAs are fixed to the stepper motors, and the motors are controlled to adjust the size of the imaging ROI. However, due to the inevitable positioning errors in the distribution of the four SUTAs, the PA signals need to be calibrated for better imaging quality. The distribute position error of the SUTAs can be divided into four cases, as shown in Figure 5. Figure 5A can be considered as the ideal distribution of the SUTA without offset errors. Figure 5B shows that the SUTA is oriented towards the imaging center, but with a backward offset error. Figure 5C illustrates the case where the SUTA is not oriented towards the imaging center. And Figure 5D shows the SUTA towards the imaging center with a forward offset error. All of the three kinds of errors in Figure 5B–D should be calibrated before image reconstruction. These errors mentioned above can be considered as signals with different delays compared with the signals received by the ideal SUTA distribution for the system. The errors illustrated in Figure 5B) can be corrected by moving the SUTA position closer to the imaging area or by shifting the signal forward. In Figure 5C, the SUTA is offset with rotation, and the transducer needs to be corrected to be oriented towards the imaging center. Alternatively, the received signal needs to be shifted according to its position to compensate for the error. For the error correction of Figure 5D, the SUTA has moved away from the imaging center, which can be calibrated by backward shifting the signals.

To test and calibrate the errors, a black spot can be placed in the center of the imaging area. After laser excitation, the PA signals can be received by the SUTAs. Figure 5E–H show the calibration signals' receiving situation of the SUTAs with distribution as shown in Figure 5A–D. The black spot is the ideal acoustic source generated in the imaging center, and the blue dots mimic the sensor distribution of the SUTA. When the SUTA position is without error, the pulse of the receiving signals will align in time series as shown in Figure 5E. When the SUTA position is with error as shown in Figure 5B–D, the calibration signals are shown in Figure 5F–H, respectively. According to the PA signals' delay analyses, the corresponding correction method can be obtained from.[19] After the SUTAs' distribution position calibration in hardware and the compensation of the data shifting, the errors can be eliminated.

In the digital domain, the relationship between data shifting bits and SUTA position error distance can be calculated as:

$$n = \frac{d}{v} \cdot f_s, \tag{2}$$

where n stands for the bit number in the digital domain of the shifting operation, d is the error of the SUTAs spatial distribution, v is the photoacoustic wave propagation speed in the medium, f_s is the data acquisition sampling rate.

After the PA signals' correction, the PA image can be reconstructed by the universal back-projection algorithms. The acoustic wave, $p(r,t)$ at position r and time t, can be described as[5, 20]:

$$\left(\nabla^2 - \frac{1}{c^2}\frac{\partial^2}{\partial t^2}\right) p(r,t) = 0. \tag{3}$$

Subject to the initial conditions:

$$p(r,t)|t=0 = \frac{\beta c^2}{C_p} A(r); \qquad \frac{\partial p(r,t)}{\partial t}|t=0 = 0 \tag{4}$$

where ∇^2 denotes the Laplacian operator, and $A(r)$ is the distribution of absorbed optical energy density. The constants β, c and C_p denote the thermal coefficient of volume expansion, speed of sound and the specific heat capacity of the medium at constant pressure, respectively. For this study, the image reconstruction requires the accurate coordinates of the transducer elements, which depend on the positions of the four SUTAs when receiving the PA wave. Figure 6 shows the coordinate calculation model of the SUTA. After getting the first quadrant SUTA's element distribution, the other coordinate can be easily got according to the symmetry. Therefore, the first quadrant transducer elements' coordinates of the SUTA can be calculated as:

$$\begin{aligned} C_x &= R \cdot \cos\theta + \frac{a - a_0}{2} \\ C_y &= R \cdot \sin\theta + \frac{a - a_0}{2}, \end{aligned} \tag{5}$$

where C_x and C_y denote the transducer element horizontal and vertical coordinates in the Cartesian coordinate system. R is the SUTA transducer's radius, θ is the transducer's angle, a and a_0 are the distance between the SUTAs defined in previous section. In this article, the parameter of R is 60 mm and a_0 is 20 mm. By applying

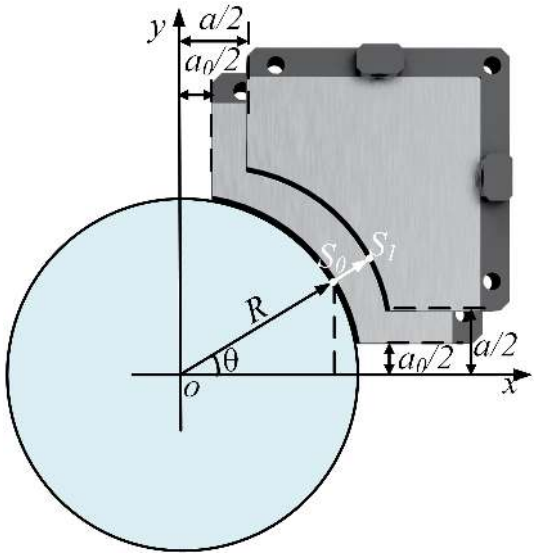

FIGURE 6 The coordinate calculating model for the first quadrant SUTA's transducer elements. θ is the angle of the transducer element, S_0 is the element position with $a = a_0$ and S_1 is the element that needs to be calculated. (The four SUTAs are arranged in the four quadrants, respectively; the original point is defined in the center of the imaging area)

Formula (5), the coordinate of the transducer array can be calculated for imaging reconstruction.

3 | SIMULATION AND EXPERIMENTAL RESULTS

3.1 | Size-adjustable ROI k-wave simulation

k-wave is a toolbox in *MATLAB*, which is designed for time-domain acoustic simulation.[21] Therefore, to demonstrate the feasibility of the proposed PAT system with ROI size-adjustable capability, we use the k-wave toolbox to simulate the different situations of the system. For the simulation setup, the SUTA is simulated with 32 sensors and linear distribution on a circular arc, whose radius is 6 mm (1/10 of the real SUTA's size). Therefore, the simulation setup can well simulate the actual design of the SUTA. The simulated sensor arrays are towards the ROI center. To simulate the proposed size-adjustable PAT setup, the SUTA sensors formed different sizes of ROI. Three kinds of distribution are simulated with small, middle and large ROI, and the parameter a denoted in Figure 3B is set as 0, 2 and 3.7 mm, respectively.

A vascular-mimicking image is used as a numerical phantom to generate PA signals by the *k-wave* toolbox simulation. To better simulate real PA signals, we assign 40 dB signal to noise ratio with an 80 MHz sampling rate. To compare the image quality between the SUTA-based PAT system and the conventional PAT system with fixed circular sensor distribution, three different sizes of the ROI are simulated. The back-projection and model-based methods are applied for image reconstruction. In the simulation setup, there are 128 sensor elements for PA signal detection. The radius of the sensors with circular distribution are 5, 6 and 7 mm, and the parameter a for the SUTA are 0, 2, and 3.7 mm.

Figure 7A,E,I are the reconstruction results by the back-projection algorithms of the small, middle and large ROI imaging of the conventional ring array ultrasound transducer. Figure 7C,G,K are the proposed size-adjustable PAT system's simulation results with different sizes by back-projection reconstruction. The small dots in the image are the sensor's distribution. Figure 7C shows the imaging result, whose parameter $a = 0$ mm. It seems to have comparable quality with the conventional fixed circle distribution, as shown in Figure 7A. For the middle size SUTA simulation result, as shown in Figure 7G, the parameter $a = 2$ mm, the outline of the phantom in this result is distinguishable. Compared with the result in Figure 7E, Figure 7G shows some artifacts due to the uncovered detection gap between SUTAs. For the large size of ROI simulation, the parameter a is set as 3.7 mm. As shown in Figure 7K, the outline of the phantom is also clear and distinguishable. However, it shows more artifacts than the result of Figure 7I corresponding to large ROI size of the circular sensor distribution. On the other hand, the gap between SUTAs will increase when the imaging size increases, which induces more severe limited view issue and artifacts. Therefore, the iterative model-based method is applied for high-quality image reconstruction. Figure 7B,F,J,D,H, I are the model-based reconstruction results corresponding to the back-projection reconstruction in Figure 7A,C,E,G,I,K, respectively. From the model-based results, it is clearly demonstrated that the SUTA-based PAT can realize high-quality imaging results as a conventional PAT system with full-ring array. Furthermore, by changing the parameter a, the SUTA-based PAT system can realize size-adjustable ROI imaging. Table 1 summarized the signal-to-noise ratio (SNR) of the simulation results of Figure 7. For nearly equal radius of the detection region, SUTA-based PAT has similar SNR with ring based PAT. With the radius increasing, the SNR declined gradually for both systems. It also shows that the MB reconstruction algorithm shows higher SNR than BP, also for both systems.

For most instances, the ultrasonic transducer array of the PAT system is nonadjustable with a fixed radius.[22] Therefore, to enhance the compatibility of the PAT system for most applications, the conventional full-ring transducer array is designed with a large radius setup.

However, due to the acoustic wave attenuation and diffraction, for the small target, the large ring array cannot receive the PA wave very well, compared with the transducer array that is closer to the target.[23] Therefore, the simulations with small-size and large-size targets are demonstrated to verify the flexibility and superiority of the SUTAs based ROI size-adjustable PAT system. Figure 8A and B are the imaging results with conventional full-ring array setup (sensor radius is 9.8 mm) for small imaging targets based on back-projection and

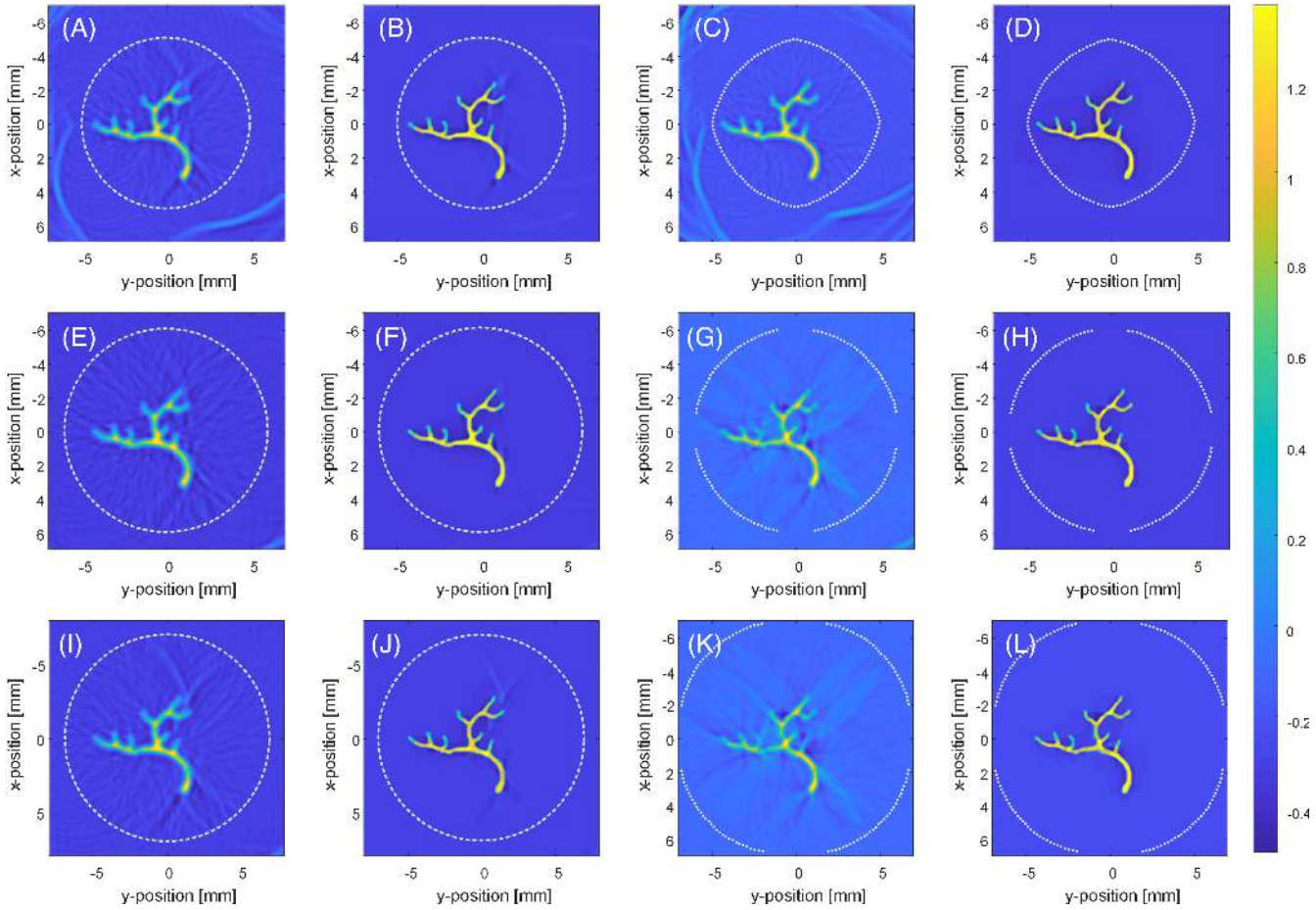

FIGURE 7 The simulation results of the size-adjustable PAT system. (A), (E) and (I) are the Back-Projection results with circular sensor distribution for different sizes targets (radius are 5, 6 and 7 mm); (B), (F) and (J) are the Model-Based reconstruction results corresponding to (A), (E) and (I) data, respectively; (C), (G) and (K) are the simulation results with Back-Projection reconstruction and the SUTA distribution (parameter $a = 0$ mm, $a = 2$ mm and $a = 3.7$ mm) with different size; (D), (H) and (L) are the Model-Based reconstruction results corresponding to (C), (G) and (K) data, respectively. (The light points are the simulation sensors distribution.)

TABLE 1 The SNR Comparison between SUTA based PAT and Ring based PAT in Figure 7

		Parameter (mm)		SNR (dB)	
Image	**Modality**	**SUTA: *a***	**Ring: *r***	**BP**	**MB**
Figure 7A,B	Ring	/	5	34.16	40.47
Figure 7C,D	SUTA	0	4.6	36.05	43.33
Figure 7E,F	Ring	/	6	33.00	38.90
Figure 7G,H	SUTA	2	6	33.08	39.84
Figure 7I,J	Ring	/	7	30.07	36.81
Figure 7K,L	SUTA	3.7	7	27.66	33.93

Abbreviations: BP, back-projection; MB, model-based; SNR, signal to noise ratio; SUTA, sectorial ultrasound transducer array.

model-based algorithms, respectively. For the small target, the large ring array cannot reconstruct a clear image shown in Figure 8A. The edge of the phantom is blurred, and some high-frequency information is lost. On the other hand, the SUTA-based imaging result shown in Figure 8C is much clearer and with a sharp outline compared with Figure 8A. For the imaging results with the model-based reconstruction algorithm, both Figure 8B, D shows satisfactory results. However, Figure 8B takes more computing resources than Figure 8D. Another disadvantage of conventional PAT system with a fixed radius full-ring array is that it cannot adjust for extra-large imaging targets. However, the proposed PAT system with SUTAs outward distribution can adapt for extra-lager phantom imaging as shown in Figure 8E (the parameter $a = 10$ mm, the equivalent full-ring array radius is 11.1 *mm*). Meantime, the transducer's limited view issue is becoming severe in Figure 8E, showing artifacts for both back-projection (Figure 8E) and model-based (Figure 8F) algorithms reconstructed images. From the result of Figure 8(F), the outline of the phantom still can be distinguished, and the target has strong contrast to the background. Furthermore, to achieve better image quality, the four SUTAs can rotate 90 degrees to get a full angle PA signals detection. Figure 8G and H are the imaging results with the four SUTAs rotating 90 degrees that equivalently forms a 256 elements UT array for PA signals' detection.

Table 2 summarized the SNR of simulation results with different sample size. For small size target in Figure 8A–D, the SUTA based PAT shows much better SNR than conventional PAT with fixed large ring in Figure 8E–H, due to its tight closure of the target. For very large size target, due to more severe limited-view

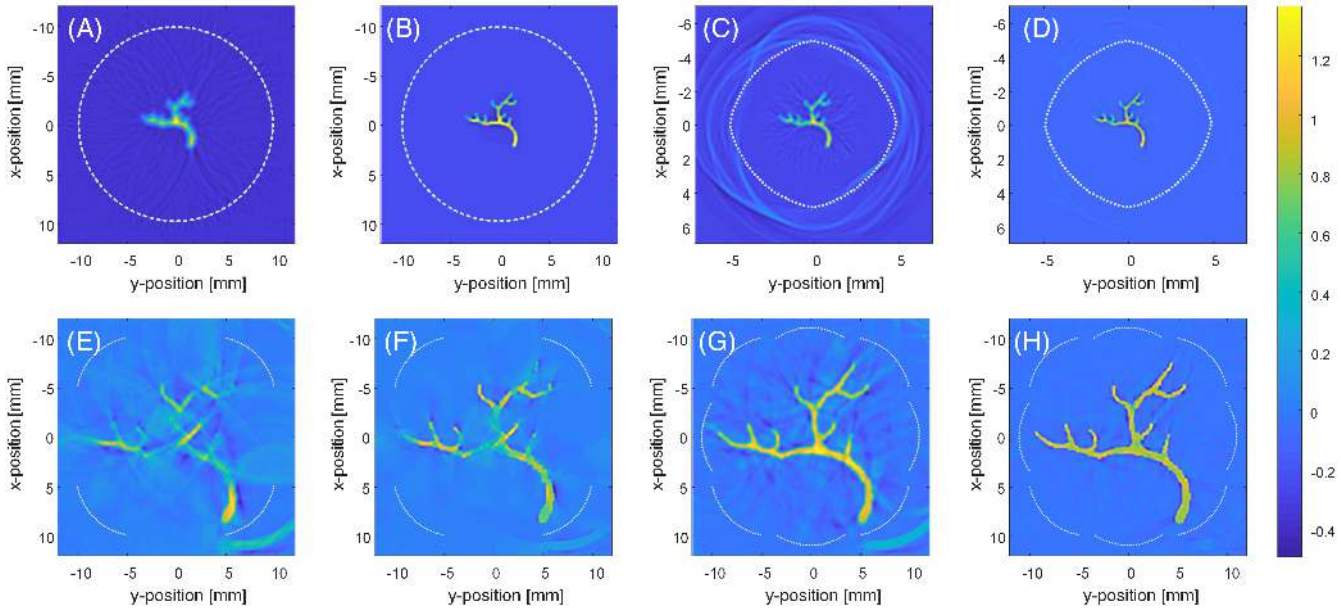

FIGURE 8 The simulation results of imaging targets with different sizes. (A) and (B) are the simulation results for small imaging targets with conventional full-ring transducer array setup (radius is 9.8 mm) reconstructed by Back-projection and Model-Based methods, respectively; (C) and (D) are the simulation results for small imaging targets with SUTAs setup (parameter $a = 0$ *mm*) reconstructed by Back-projection and Model-Based methods, respectively; (E) and (G) are the Back-projection results for large target corresponding to with and without rotation (parameter $a = 10$ *mm*); (F) and (H) are the Model-Based reconstruction results corresponding to results in (E) and (G)

TABLE 2 The SNR comparison of targets with different sizes

		Parameter		SNR (dB)	
Image	**Modality**	***a/r* (mm)**	**elements**	**BP**	**MB**
Figure 8A,B	Ring	9.8	128	14.12	30.74
Figure 8C,D	SUTA	0	128	31.61	35.59
Figure 8E,F	SUTA	10	128	15.50	25.33
Figure 8G,H	SUTA	10	256	23.79	29.28

Abbreviations: BP, back-projection; MB, model-based; SNR, signal to noise ratio.

issue, image SNR of SUTA based PAT declines (Figure 8 (E,F). To solve this issue by rotating the four SUTA transducers, the SNR of the image can be greatly enhanced (Figure 8G,H).

The field of view formed by the four SUTAs varies with the parameter a, which is shown in Table 3. The parameter r is the radius of the inscribed circle calculated by Formula (1). With a increasing, the full view percentage of SUTAs scanning declines. It is worth noting that the SUTAs can realize 360° full field of view by 45° rotation for all these cases in Table 3. For different scanning schemes of the four SUTAs, the sensitivity maps are shown in Figure 9.

TABLE 3 The field of view of the SUTA with different sizes

a (mm)	*r* (mm)	Angle	Full view percentage (%)
0	46	360°	100
20	60	283.2°	78.7
30	65.9	254.8°	70.8
40	72	231.1°	64.2
50	78.3	211°	58.6
60	84.7	194°	53.9

3.2 | The PAT system setup with SUTAs

The phantom study is executed to demonstrate the feasibility of the proposed size-adjustable PAT system. The PAT system with SUTAs with photograph is shown in Figure 10. The laser source (PHOCUS MOBILE, OPOTek Inc., USA) with 10 Hz repetition rate, 750 nm wavelength and 70 mJ energy, is used to excite the phantom to generate PA signal. The four SUTAs form a 128-elements array to capture the PA signal. A 128-channel data acquisition (DAQ) module with 40 MHz sampling rate is applied for PA signal sampling (LEGION 128 ADC, PhotoSound Technologies, Inc., USA). There are four stepper motors

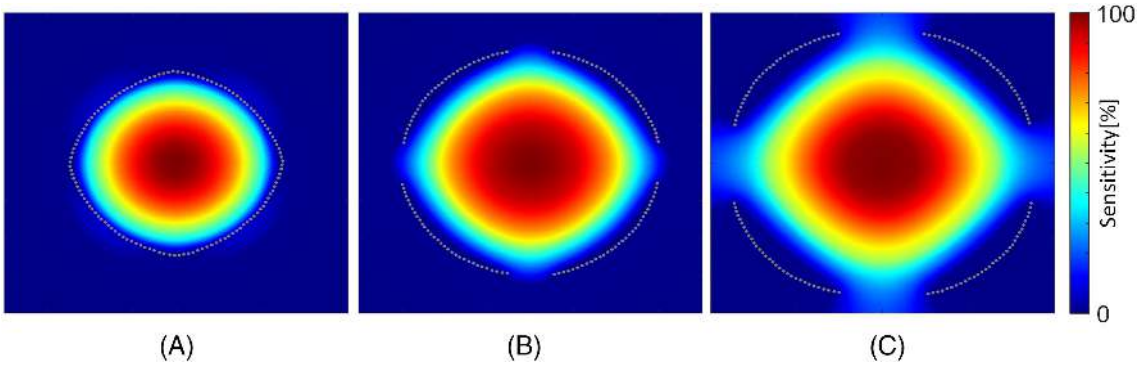

FIGURE 9 The simulated sensitivity map of various distribution of the SUTAs. (A), (B) and (C) stand for the small, middle and large field of view scanning schemes, respectively (parameter $a = 0$, 20 and 40 mm)

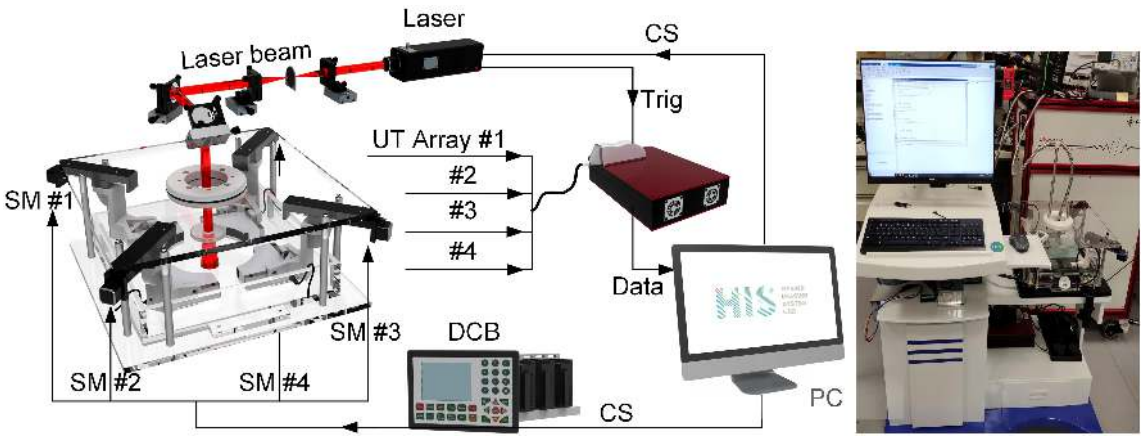

FIGURE 10 The proposed size-adjustable PAT system setup and its photograph. #, device number; CS, control signal; DCB, digital control board; PC, personal computer; SM, stepper motor; Trig, trigger; UT, ultrasound transducer

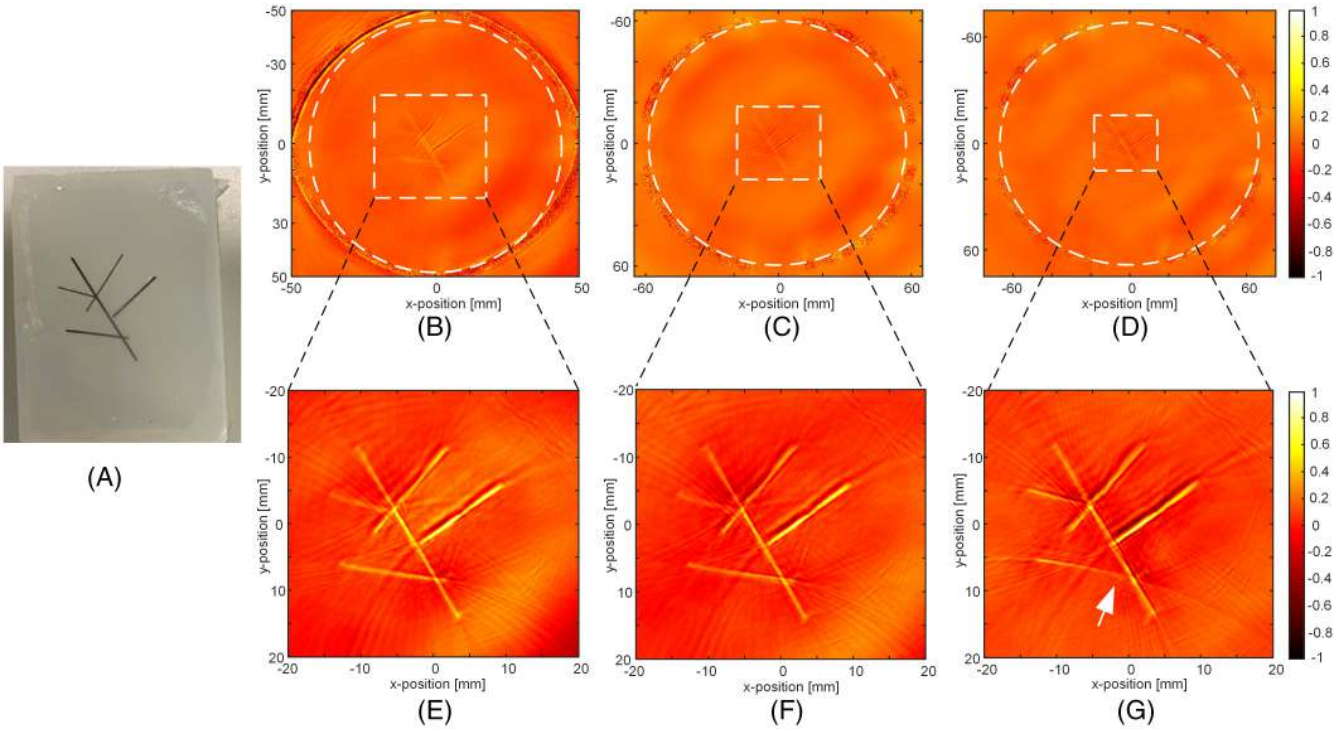

FIGURE 11 The phantom imaging results. (A) the photograph of the phantom; (B), (C) and (D) are the top view of imaging results corresponding to $a = 0$ mm, $a = 20$ mm and $a = 35$ mm with different imaging sizes; (E), (F) and (G) are the region of interest of the imaging results corresponding to the (B), (C) and (D), respectively

TABLE 4 The SNR of phantom imaging results

Image	SUTA: a (mm)	r (mm)	SNR (dB)
Figure 11E	0	46	34.16
Figure 11F	20	60	30.07
Figure 11G	35	69	27.66

Abbreviations: SNR, signal to noise ratio; SUTA, sectorial ultrasound transducer array.

fixed in a custom-shaped acrylic platform that ensures the four SUTAs towards the imaging center when the motors are moving. A digital control board includes four stepper motor drivers, and a controlling module that controls the movement of the motor. By doing so, the SUTAs can dynamically adjust the size of imaging ROI. The imaging target is surrounded by the four SUTAs ensuring that the PA signals can be well detected. The laser homogeneously excited on the imaging phantom after some optical components' adjustment. Meanwhile, the laser clock module outputs the synchronous trigger to the DAQ. After that, the computer reconstructs the PA image by applying universal back-projection algorithms.[11, 24]

3.3 | Size-adjustable PAT experiments

The imaging sample is blood vessel-like phantom, which has pencil leads with 0.38 and 0.5 mm diameter embedded in an agar block as shown in Figure 11A. Figure 11B–D are the top view of imaging results corresponding to $a = 0$ mm, $a = 20$ mm and $a = 35$ mm with different ROIs. The corresponding zoom-in images are shown in Figure 11E–G. Table 4 summarizes the SNR of the phantom imaging results, showing that SUTA closer to the imaging target gives better SNR. Figure 11E–G are the imaging results by the Back-projection algorithms of the phantom corresponding to $a = 0$ mm, $a = 20$ mm and $a = 35$ mm with different imaging ROI. The imaging results verified the feasibility of the proposed size-adjustable PAT system to adapt for different sizes' targets by changing the SUTAs distribution. Although with the imaging size increasing, the limited-view induced artifacts also increase in the imaging result, the imaging result can be improved by signals interpolation and image processing.[25, 26] Therefore, the PAT system based on SUTAs is more flexible for imaging targets with different sizes, compared with the conventional PAT system with a fixed circular distribute UT array.

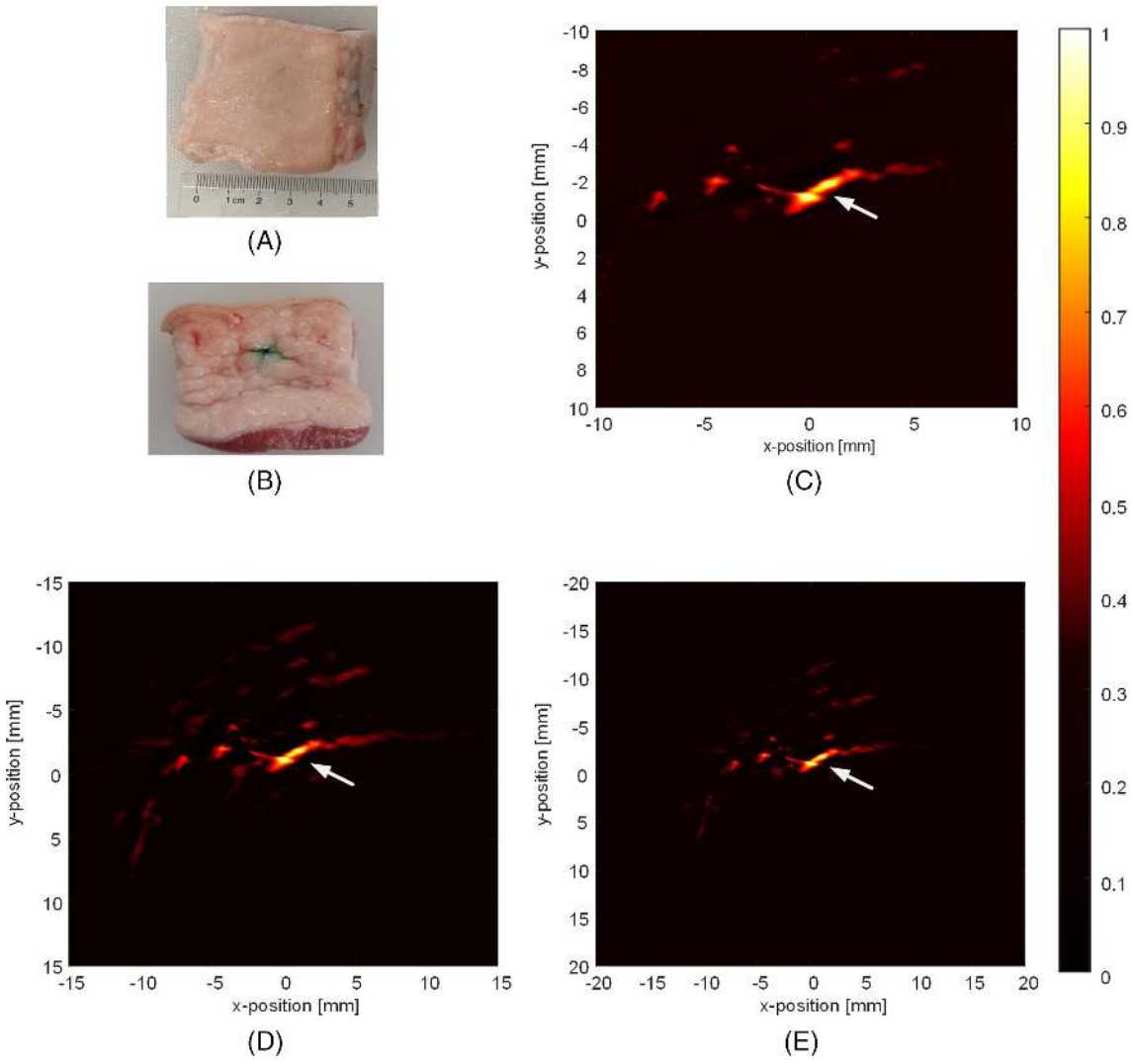

FIGURE 12 The ex-vivo imaging results. (A) the photograph of the pork breast; (B) the lateral view of the pork breast with ICG injections; (C–E) the imaging results with various sizes of imaging region corresponding to 20 × 20 mm^2, 30 × 30 mm^2 and 40 × 40 mm^2 view, respectively; the white arrow indicating the injected ICG

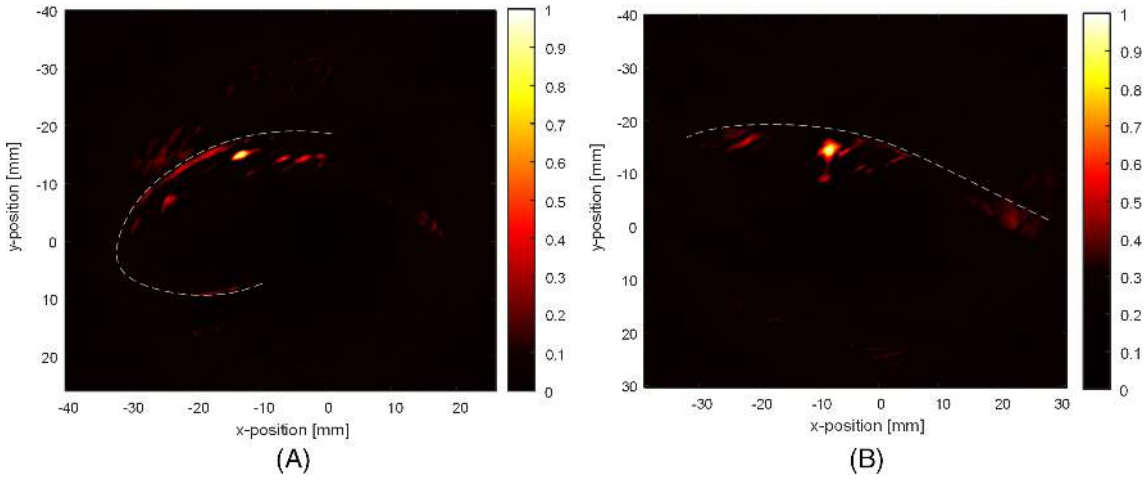

FIGURE 13 The human in-vivo imaging results. (A) the imaging result of the right wrist and (B) the imaging results of the right ankle

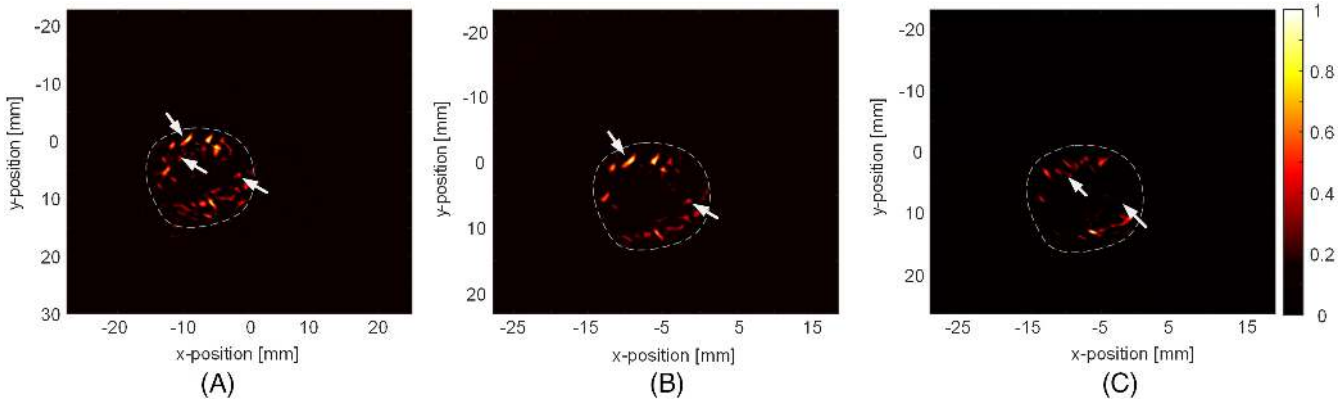

FIGURE 14 The human finger imaging results with multiple frequencies reconstruction. (A) the imaging result with multiple frequency PA signals; (B) the imaging result with low frequency (center frequencies are 1 and 2.5 MHz) PA signals; (C) the imaging result with high frequency (center frequencies are 5 and 7.5 MHz) PA signals (the white dashed line marks the surface of skin)

3.4 | Ex-vivo and in-vivo imaging

An ex-vivo pork breast with ICG injection is imaged by the proposed PAT system, which verified its feasibility for biomedical applications. The ex vivo pork breast phantom composed by skin, fat and capillaries etc., can very well simulate the real biological tissue scenarios. Figure 12A and B are the photographs of the ex-vivo pork breast meat. The contrast agent Indocyanine Green (ICG) (Dandong Yichuang Pharmaceutical Co. Ltd.) is injected at a depth of 2 to 3 cm under the skin of the phantom. Figure 12B shows the lateral view of the phantom after injection. ICG is an FDA-approved contrast agent for PA signal enhancement in deep tissue. The wavelength of the laser is selected to be 780 nm that matches the ICG's maximum absorption wavelength. The fluence of the laser is <20 mJ/cm^2 at the skin surface within the safety limit. Figure 12C–E shows the ex-vivo imaging results with various sizes of imaging region corresponding to 20×20 mm^2, 30×30 mm^2 and 40×40 mm^2 views, respectively, where the bright target with high contrast to the background is the injected ICG, Other high-intensity spots are the blood vessel cross-section, because blood in the pork breast also generated PA signal after light excitation. The average SNR of the imaging results is 36.56 dB.

The proposed system is also validated to image blood vessels of human wrist and ankle that verified its flexibility to adapt for various size's targets. The laser source is selected as 1064 nm (LPS-1064-L, CNI, China) for better light penetration. Figure 13 shows the in-vivo imaging results. Figure 13A,B corresponds to the blood vessel imaging results of the inside right wrist and ankle, respectively. The white dashed line marks the surface of skin. The cross-sections of the blood vessels are obviously identified with high contrast to the background.

The human finger imaging results are demonstrated for multiple frequencies analysis shown in Figure 14. Figure 14A is reconstructed by multiple frequencies' PA signals, which shows details of the thick and thin blood vessels' cross-section. Figure 14B andC are reconstructed images corresponding to the low frequency and high frequency PA signals. The arrows denote some different details of the imaging results, which demonstrated the advantages of the multiple frequencies for image reconstructions.

4 | DISCUSSION

In this research, the proposed SUTA-based PAT system with size-adjustable ROI imaging can adapt for targets with different sizes. The parameter a can quantitatively analyze the size of ROI. Based on Equation (1), we can calculate the system's equivalent radius. Compared with the conventional ring array with a fixed radius, the SUTA-based PAT system is the first demonstration of the ring-shape PAT system that enables adjusting the radius of the ROI. The proposed system enables tight enclosure of the sample by tuning the radius of the four sectorial transducers, which improves the image quality by reducing acoustic attenuation, for example, using large-ring to image small sample will cause severe acoustic attenuation/distortion during the acoustic propagation. Moreover, four separated sectorial transducers enable flexibility of assigning different frequency to each transducer. The coverage angles of the transducer element are different for different center frequencies. For small field of view imaged by the four SUTAs with different center frequencies, the reconstructed image is with satisfactory performance. With the imaging region increasing, the limited view and acoustic diffractions

affect the imaging quality and induce some artifacts. Therefore, by rotating these transducers, it equivalently achieves larger-bandwidth ultrasonic detection that can greatly enhance image quality, meanwhile eliminating the angle coverage issue.

The SUTAs with different center frequencies can capture the PA signals with equivalently much wider bandwidth, which can restore the PA signal with higher fidelity. The previous literature also shows that PA signal with multi-frequency/bandwidth can enhance PA image reconstruction greatly.[7] Regarding the attenuation compensation for SUTAs with different frequencies and ROIs, one possible way to address this issue is to calibrate the attenuation coefficient for each transducer and each typical size of ROIs, before the imaging operation. Based on the attenuation calibration, the received signals can be compensated for better image reconstruction. It is worth mentioning that the attenuation compensation and error calibration can be automatically accomplished during the imaging procedure by loading the pre-measured parameters. Moreover, calculating the SUTA actual coordinate for BP reconstruction is another solution to compensate the attenuation and calibrate the errors.

The simulation results very well demonstrated the feasibility of the proposed size-adjustable PAT system. It deserves mentioning that there are increasing artifacts in the imaging results when the equivalent radius increases due to the limited-view issue. The four SUTAs with rotational scanning can not only address the limited-view issue by fully covering the target, but also capture the PA signals with multi-frequency from all directions for better PAT imaging quality.

For further research of the SUTA-based PAT system, the SUTA and the light illumination design will be integrated into a moveable bed for clinical human breast imaging. The SUTA will change the size of the imaging region to adapt to the various sizes of the breast. The SUTA will move close to the imaging target to get optimized acoustic coupling and high SNR. Additionally, the SUTA with elevating motor can realize a cylindrical scanning for 3D PAT imaging, the imaging size can be dynamically adjusted in real-time for each imaging cross-section, which enables the PAT system for clinical applications such as human breast and ankle imaging. Furthermore, the SUTA-based PAT system with model-based image reconstruction algorithms can further improve imaging quality.

5 | CONCLUSION

In this article, the size-adjustable PAT system is proposed that can adapt to different sizes' imaging targets. This system greatly improves the flexibility of the PAT system for biomedical applications. Specifically, the proposed system can apply for human breast cancer imaging with different sizes to achieve optimum imaging performance. The SUTAs with different center frequencies can detect the PA signals with a wider spectrum and higher fidelity. The size-adjustable PAT system is based on the SUTAs distribution that can be motorized to adjust the imaging ROI. The four SUTAs can adjust the imaging ROI's radius ranging from 50 to 100 mm. For extra-large target, rotating the four SUTAs can form an equivalent 256 channels' UT array to compensate the signal detection limited view issue. A calibration processing of the PA signals should be carried out before applying the reconstructions algorithms.

Simulation and experimental results of a vascular model have well demonstrated the feasibility of the proposed PAT system with the SUTAs. Moreover, further advanced signal and image processing algorithms can be used to improve imaging quality. The proposed system shows high potential to promote the PAT system for wider clinical applications with enhanced flexibility, especially in cancer screening.

DATA AVAILABILITY STATEMENT

Data available on request from the authors

ORCID

Fei Gao https://orcid.org/0000-0001-7524-1499

REFERENCES

[1] L. Nyström, I. Andersson, N. Bjurstam, J. Frisell, B. Nordenskjöld, L. E. Rutqvist, *Lancet (London, England)* **2002**, *359*(9310), 909.

[2] L. V. Wang, S. Hu, *Science* **2012**, *335*, 1458.

[3] L. V. Wang, J. Yao, *Nat. Methods* **2016**, *13*(8), 627.

[4] L. V. Wang, *IEEE J. Select Top. Quant. Electron.* **2008**, *14* (1), 171.

[5] C. Li, L. V. Wang, *Phys. Med. Biol.* **2009**, *54*, R59.

[6] H. Li, B. Dong, Z. Zhang, H. F. Zhang, C. Sun, *Sci. Rep.* **2014**, *4*, 4496.

[7] G. Ku, X. Wang, G. Stoica, L. V. Wang, *Phys. Med. Biol.* **2004**, *49*, 1329.

[8] G. Paltauf, P. Hartmair, G. Kovachev, R. Nuster, in *SPIE Proceedings. Opto-Acoustic Methods and Applications in Biophotonics III, Munich*, Vol. 10415 (Ed: V. Ntziachristos), Optical Society of America, Washington, DC **2017**, p. 1041509.

[9] N. Nyayapathi, J. Xia, *J. Biomed. Opt.* **2019**, *24*(12), 1.

[10] N. Nyayapathi, R. Lim, H. Zhang, W. Zheng, Y. Wang, M. Tiao, K. W. Oh, X. C. Fan, E. Bonaccio, K. Takabe, J. Xia, *IEEE Trans. Biomed. Eng.* **2020**, *67*(5), 1321.

[11] M. Xu, L. V. Wang, *Phys. Rev. E Stat. Nonlin. Soft Matter Phys.* **2005**, *71*, 016706.

[12] S. Manohar, M. Dantuma, *Photoacoustics* **2019**, *16*, 100134.

[13] Z. Xie, F. M. Hooi, J. B. Fowlkes, R. W. Pinsky, X. Wang, P. L. Carson, *Ultrasound Med. Biol.* **2013**, *39*(11), 2176.
[14] Y. Matsumoto, Y. Asao, H. Sekiguchi, A. Yoshikawa, T. Ishii, K.-i. Nagae, S. Kobayashi, I. Tsuge, S. Saito, M. Takada, Y. Ishida, M. Kataoka, T. Sakurai, T. Yagi, K. Kabashima, S. Suzuki, K. Togashi, T. Shiina, M. Toi, *Sci. Rep.* **2018**, *8*(1), 14930.
[15] L. Lin, P. Hu, X. Tong, S. Na, R. Cao, X. Yuan, D. Garrett, J. Shi, K. Maslov, L. Wang, *Nat. Commun.* **2021**, *12*(1), 882.
[16] D. Jiang, H. Lan, Y. Xu, Y. Wang, F. Gao, F. Gao, presented at 2021 IEEE Int. Symp. Circ. Syst. (ISCAS) **2021**.
[17] S. Bu, Z. Liu, T. Shiina, K. Kondo, M. Yamakawa, K. Fukutani, Y. Someda, Y. Asao, *IEEE Trans. Biomed. Eng.* **2012**, *59*(5), 1354.
[18] M. Xu, L. Wang, *Rev. Sci. Instrum.* **2006**, *77*, 041101.
[19] D. Jiang, H. Lan, H. Zhong, Y. Zhao, H. Li, F. Gao, *IEEE Trans. Circ. Syst. II Expr. Briefs* **2019**, *66*(5), 778.
[20] K. Wang, M. A. Anastasio, *Phys. Med. Biol.* **2012**, *57*(23), N493-9.
[21] B. E. Terrby, B. T. Cox, *J. Biomed. Opt.* **2010**, *15*(2), 021314.
[22] J. Xia, M. R. Chatni, K. Maslov, Z. Guo, K. Wang, M. Anastasio, L. V. Wang, *J. Biomed. Opt.* **2012**, *17*(5), 050506.
[23] J. L. M. M. S. Greenwood, M. S. Good, *J. Acoust. Soc. Am.* **1993**, *94*, 908.
[24] J. Xiao, X. Luo, K. Peng, B. Wang, *Appl. Opt.* **2017**, *56*(32), 8983.
[25] D. van de Sompel, L. S. Sasportas, J. V. Jokerst, S. S. Gambhir, *PLoS One* **2016**, *11*(3), e0152597.
[26] A. A. Oraevsky, L. V. Wang, presented at the Photons Plus Ultrasound: Imaging Sens. **2018**.

How to cite this article: D. Jiang, Y. Xu, H. Lan, Y. Shen, Y. Zhang, F. Gao, L. Liu, F. Gao, *J. Biophotonics* **2022**, *15*(7), e202200070. https://doi.org/10.1002/jbio.202200070